C. R. Geoscience 351 (2019) 80–85

Contents lists available at ScienceDirect

Comptes Rendus Geoscience

www.sciencedirect.com

Internal Geophysics (Physics of Earth's Interior)

Olivine intergranular plasticity at mantle pressures and temperatures

Paul Raterron [a,*], Caroline Bollinger [b], Sébastien Merkel [a]

[a] Unité "Matériaux et Transformation" (UMET), CNRS, Université Lille-1, 59655 Villeneuve-d'Ascq cedex, France

ARTICLE INFO

Article history:
Received 2 March 2018
Accepted after revision 9 October 2018
Available online 18 March 2019

Handled by Robert C. Liebermann

Keywords:
Olivine
Plasticity
High-pressure
Intergranular
Upper mantle

ABSTRACT

The ductile behavior of olivine-rich rocks is critical to constrain thermal convection in the Earth's upper mantle. Classical olivine flow laws for dislocation or diffusion creep fail to explain the fast post-seismic surface displacements observed by GPS, which requires a much weaker lithosphere than predicted by classical laws. Here we compare the plasticity of olivine aggregates deformed experimentally at mantle pressures and temperatures to that of single crystals and demonstrate that, depending on conditions of stress and temperature, strain accommodated through grain-to-grain interactions – here called intergranular strain – can be orders of magnitude larger than intracrystalline strain, which significantly weakens olivine strength. This result, extrapolated along mantle geotherms, suggests that intergranular plasticity could be dominant in most of the upper mantle. Consequently, the strength of olivine-rich aggregates in the upper mantle may be significantly lower than predicted by flow laws based on intracrystalline plasticity models.

Published by Elsevier Masson SAS on behalf of Académie des sciences. This is an open access article under the CC BY-NC-ND license (http://creativecommons.org/licenses/by-nc-nd/4.0/).

[b] Bayerisches Geoinstitut, University of Bayreuth, 95440 Bayreuth, Germany

1. Introduction

The plasticity of olivine-rich rocks constraints that of Earth's upper mantle. Consequently, there has been considerable effort to quantify olivine aggregate rheology in terms of flow laws that can be implemented in geodynamical models for mantle thermal convection. Experimental studies investigated the effects of temperature and stress (see review in Hirth and Kohlstedt, 2003), pressure (e.g., Bollinger et al., 2013; Durham et al., 2009; Hilairet et al., 2012), fluid fugacities (e.g., Keefner et al., 2011; Kohlstedt, 2006; Ohuchi et al., 2017), grain size (Warren and Hirth, 2006), lattice-preferred orientations (e.g., Hansen et al., 2013), and melt fractions (e.g., Hirth and Kohlstedt, 1995). The traditional view is to assign one dominant deformation mechanism to given deformation conditions (Frost and Ashby, 1982) and implement the flow law with specific dependences on temperature, stress, or grain size. At the microscopic scale, however, olivine aggregate plasticity involves numerous mechanisms operating concurrently, within the grains and at grain-boundary (Fig. 1). To this day, the fundamental question of the amount of strain accommodated in the mantle through grain-to-grain interactions versus that accommodated within the grain remains unanswered.

Strain accommodation at grain boundaries has been attributed to several distinct mechanisms. A model for the deformation of aggregates by grain-boundary diffusion was introduced by Coble (1963) to explain the high-temperature plasticity of alumina. Coble creep requires the rearrangement of grain interfaces by grain-boundary

* Corresponding author. The National Science Foundation, 2415 Eisenhower Avenue, Alexandria, VA 22314, USA.
E-mail address: praterro@nsf.gov (P. PaulRaterron).

https://doi.org/10.1016/j.crte.2018.10.001
1631-0713/Published by Elsevier Masson SAS on behalf of Académie des sciences. This is an open access article under the CC BY-NC-ND license (http://creativecommons.org/licenses/by-nc-nd/4.0/).

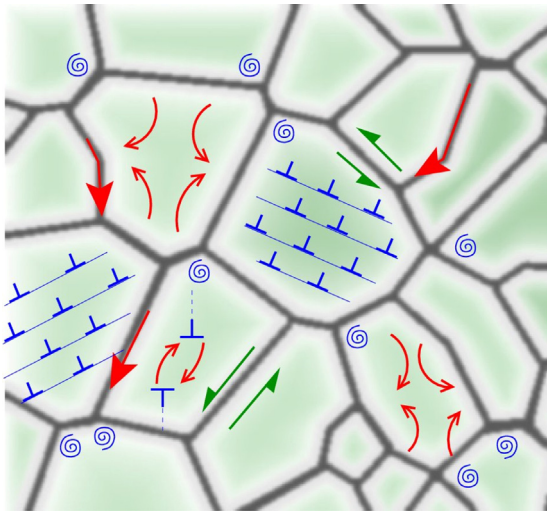

Fig. 1. Schematics of mechanisms accommodating strain in olivine aggregates: dislocations (blue corners) glide, cross slip and climb within grains, disclinations [blue spirals, Cordier et al. (2014)] mostly active near grain boundaries, ionic diffusion (red arrows) occurring at grain interfaces (Cobble diffusion) or within the grains (Nabarro–Herring diffusion, dislocation climb), and grain-boundary sliding (green arrows, see Hansen et al., 2011), which also involves diffusion and can be assisted by dislocations. Other mechanisms that do not accommodate strain, such as grain-boundary migration or recrystallization, also assist olivine deformation.

sliding (GBS). The corresponding flow law exhibits a linear dependence on stress and a strong inverse dependence on grain size (d), theoretically to the power $p = -3$. For persistently small grain sizes – when grain growth is, for example, impeded by Zener pinning – Coble creep may contribute to superplastic flow, which has been characterized at room pressure in olivine-rich aggregates (e.g., Hiraga et al., 2010). Grain-boundary sliding can also be assisted by dislocation motions within grains, which contribute to relax stress concentration at triple junctions. This mechanism, called dislocation-assisted grain-boundary sliding (disGBS), has been observed at low pressure in olivine (Hansen et al., 2011; Hirth and Kohlstedt, 2003). It is characterized by a strain rate depending strongly on stress, typically to the power $n \sim 3$, with an inverse dependence on grain size to a power p within $[-2, -0.6]$. Other deformation mechanisms, which do not exist in single crystals, accommodate strain in olivine aggregates. Motions of disclinations – defects identified along grain boundaries in olivine (Cordier et al., 2014) – can accommodate strain. Furthermore, interactions between grains, in materials with limited number of intracrystalline deformation mechanisms, generate locally high stress concentrations (e.g., Castelnau et al., 2008). In materials with anisotropic elastic and plastic properties such as olivine, this may promote high stress and strain transmission patterns percolating throughout the aggregates (Burnley, 2013). Conversely, the stress field associated with single crystal deformation can only be relaxed by intracrystalline deformation mechanisms, such as dislocation motions (glide, climb and cross slip) and intracrystalline diffusion (e.g., Nabarro–Herring diffusion).

Recently, Tielke et al. (2016) compared olivine single crystal and aggregate high-temperature rheology at low pressure, and quantified the contribution of both intracrystalline and intergranular mechanisms to the aggregate strain. They determine that olivine aggregates deform up to 4.6 times faster than what would be expected assuming only intracrystalline plasticity; the latter's contribution to strain rate was calculated from micromechanical modeling of dislocations activity. Following a similar approach, we here compare olivine single crystal and aggregate high-temperature plasticity, as measured experimentally at the high-pressures representative of mantle conditions. We demonstrate that grain-to-grain interactions significantly contribute to accommodating strain in experiments. Extrapolation to mantle stress conditions along geotherms suggests that intergranular plasticity may also dominate upper mantle plasticity.

2. Methods intracrystalline vs. intergranular plasticity

Comparing aggregates and single crystal deformation data allows quantifying the strain rate contributions of intergranular deformation mechanisms. Assuming that intracrystalline (IC) and intergranular (IG) mechanisms operate concurrently, we have:

$$\dot{\epsilon}_{Agg} = \dot{\epsilon}_{IC} + \dot{\epsilon}_{IG} \quad (1)$$

where $\dot{\epsilon}_{Agg}$ is the strain rate of the aggregate, $\dot{\epsilon}_{IC}$ is the contribution of intracrystalline processes and $\dot{\epsilon}_{IG}$ is due to grain-to-grain interactions. The plasticity of aggregates can thus be quantified by introducing the following ratio:

$$\dot{\epsilon}_{Agg}/\dot{\epsilon}_{IC} = 1 + \dot{\epsilon}_{IG}/\dot{\epsilon}_{IC} \quad (2)$$

It should range from 1, when all the aggregate strain is accommodated within the grains, to $+\infty$, when the strain is fully accommodated through grain-to-grain deformation processes. Values for $\dot{\epsilon}_{Agg}$ and $\dot{\epsilon}_{IC}$ (and their ratio $\dot{\epsilon}_{Agg}/\dot{\epsilon}_{IC}$) can be directly extracted from previously published rheological data (Fig. 2).

We used $\dot{\epsilon}_{Agg}$ values for San Carlos olivine aggregates deformed in axisymmetric compression at mantle pressure and temperature in the Deformation-DIA (D-DIA) apparatus, as reported by Durham et al. (2009), Hilairet et al. (2012), and Bollinger et al. (2013) – see supplementary Table S1. For each $\dot{\epsilon}_{Agg}$ reported value, the corresponding $\dot{\epsilon}_{IC}$ can be calculated at identical pressure (P), temperature (T), and differential stress (σ) by combining experimental flow laws for San Carlos olivine single crystals (Bai et al., 1991; Girard et al., 2013; Mackwell et al., 1985; Raterron et al., 2009) – see supplementary material, Table S2. Indeed, assuming homogeneous stress throughout the aggregate (lower bound approach, i.e. Sachs' bound) – one of the simplest end-member assumption when analytically addressing aggregate strain – and random grain orientations in the aggregate, $\dot{\epsilon}_{IC}$ becomes:

$$\dot{\epsilon}_{IC} = 0.123\left(\dot{\epsilon}_{[110]C} + \dot{\epsilon}_{[011]C} + \dot{\epsilon}_{[101]C}\right) \quad (3)$$

where $\dot{\epsilon}_{[110]C}$, $\dot{\epsilon}_{[011]C}$, and $\dot{\epsilon}_{[101]C}$ are the strain rates of oriented single crystals and the 0.123 geometrical factor

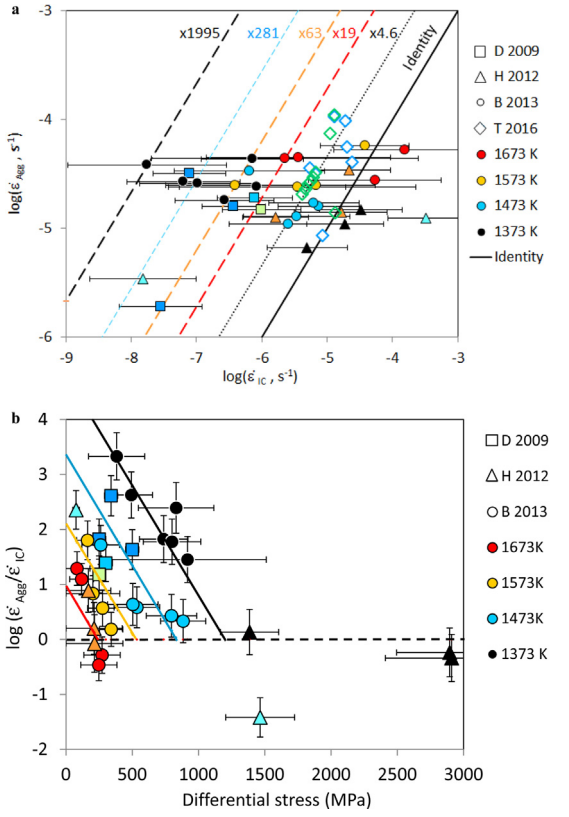

Fig. 2. a: aggregate strain rate ϵ_{Agg} as measured in experiments (Table S1) versus predictions based on the intracrystalline strain rate ϵ_{IC} as calculated from the parameters in Eq. (3) and Table S2. The color code indicates experimental temperatures. D, H, and B are data from Durham et al. (2009), Hilairet et al. (2012), and Bollinger et al. (2013), respectively. Also shown are the data reported by Tielke et al. (2016) (*T*; open diamond, green is for 1523 K): for these data, shear strain rates and stresses were converted into compressional strain rates and stresses. The thick black line is identity, for which both strain rates are equal. Dotted and dashed lines indicate ratios for which the aggregate strain rate is 4.6 (dotted black), 19 (red), 63 (orange), 281 (blue), and 1995 (dashed black) times faster than the intracrystalline strain rate; b: $\log(\epsilon_{Agg}/\epsilon_{IC})$ versus experimental differential stress; the colored lines are the results of a bilinear fit in T and σ through the data (Eq. (4)); their color indicates temperature.

arises from averaging over crystal orientations (Raterron et al., 2011). The indexes indicate the crystallographic orientation of the compression direction – e.g., the $[110]_c$ direction is at a 45° angle from the [100] and [010] directions. The $[110]_c$, $[011]_c$, $[101]_c$ directions promote respectively [100](010) dislocation slip, [001](010) dislocation slip, and [100](001) and [001](100) slips together. The single crystal strain rates $\epsilon_{[110]C}$, $\epsilon_{[011]C}$, and $\epsilon_{[101]C}$ account for pressure, temperature, water content, and oxygen fugacity f_{O_2} and are based on data from the literature (see Supplementary Information). For the dry experiments reported by Durham et al. (2009) (squares in Fig. 2), we assumed a dry-crystal rheology when calculating ϵ_{IC}; for the wet experiments reported by Hilairet et al. (2012) and Bollinger et al. (2013) (triangles and circles in Fig. 2), we assumed wet-crystal rheology. ϵ_{IC} was also calculated assuming oxygen fugacity conditions comparable to those of the experiments. For Durham et al.'s (2009) experiments, where the Ni/NiO buffer controlled f_{O_2}, we assumed the Ni/NiO buffer oxygen fugacity (Frost, 1991). For the unbuffered experiments (Bollinger et al., 2013; Hilairet et al., 2012) – where oxygen fugacity was not controlled but specimens were placed within a boron nitride sleeve that promotes low-f_{O_2} conditions (Wendland et al., 1982) – we assumed the oxygen fugacity of the iron – wüstite buffer (IW) that borders the olivine stability field.

3. Results aggregate strain rate $\dot{\epsilon}_{Agg}$ versus intracrystalline strain rate $\dot{\epsilon}_{IC}$

Fig. 2a shows the aggregate strain rate ϵ_{Agg}, as measured experimentally (Table S1), versus the intracrystalline strain rate ϵ_{IC} (Eq. 3) calculated at identical P, T, and σ. Because of our initial assumption (Sachs' bound), Eq. (3) tends to overestimate the intracrystalline strain rate. This may occasionally lead to $\epsilon_{Agg} < \epsilon_{IC}$ when strain is fully accommodated by intracrystalline processes. Remarkably, we have $\epsilon_{Agg} \geq \epsilon_{IC}$ (within uncertainty) for all but one experimental point, by factors reaching ~20 at 1673 K and ~2000 at 1373 K. This shows that, in high-pressure deformation experiments, (*i*) a significant fraction of aggregate strain is accommodated by mechanisms involving grain-to-grain interactions, even in regimes where dislocation creep was observed. It also shows that (*ii*) this fraction tends to increase with decreasing temperature. Also shown in Fig. 2a are the data reported by Tielke et al. (2016) obtained at low pressure (open diamonds, green is for 1523 K). For these data, shear strain rates and stresses were converted into compressional strain rates and stresses before plotting. Tielke et al. report that the aggregate strain rate is up to 4.6 times the intracrystalline strain rate as calculated using a micromechanical modeling; Fig. 2a shows that these data fall, indeed, in the vicinity of the line corresponding to a ratio of 4.6 between the measured strain rate and the intracrystalline strain rates calculated here using the analytical approach described above. It is remarkable that using two different approaches, Tielke et al. and we obtained similar results. This give us confidence in the analytical approach used here.

Fig. 2b shows $\log(\epsilon_{Agg}/\epsilon_{IC})$ versus stress; the color code indicates approximate temperatures. The ratio $\epsilon_{Agg}/\epsilon_{IC}$ varies over orders of magnitude, from ~1 to $\sim 2 \times 10^3$. When $\epsilon_{Agg}/\epsilon_{IC} \sim 1$ the aggregate strain is fully accommodated within the grains, while $\epsilon_{Agg}/\epsilon_{IC} \gg 2$ indicates that strain is mostly accommodated by grain-to-grain interactions (intergranular mechanisms). Within our model, one should always satisfy $\epsilon_{Agg}/\epsilon_{IC} \geq 1$ (Eq. (2)), which, within uncertainties, is in agreement with most experimental data. At a given temperature, $\log(\epsilon_{Agg}/\epsilon_{IC})$ decreases with increasing differential stress (Fig. 2b) until $\log(\epsilon_{Agg}/\epsilon_{IC}) \sim 0$ is achieved, i.e. strain is fully accommodated within the grains $(\epsilon_{Agg} = \epsilon_{IC})$. A further increase of stress will have no effect on the ratios in Eq. (2). This result is in agreement with the conventional interpretation that increasing stress and strain rate at given temperature favors dislocation creep (Frost and Ashby, 1982) – a grain size insensitive creep involving mostly intracrystalline

plasticity – with respect to grain size sensitive creep, which involves intergranular plasticity.

The contribution of grain-to-grain deformation processes to the aggregate strain also decreases with temperature (Fig. 2a and b). This effect may result from a combination of factors, such as an increasing aggregate grain size with temperature, i.e. a decreasing grain-boundary surface/bulk volume ratio favoring intracrystalline deformation mechanisms, an increasing activity of disclinations with decreasing T favoring intergranular plasticity, higher stress and strain concentrations near grain boundaries at lower T, or a more effective stress percolation at moderate T (Burnley, 2013) promoting high-strain networks throughout the aggregates, accounted here for as intergranular strain.

A linear fit through $\log(\epsilon_{Agg}/\epsilon_{IC})$ in Fig. 2b leads to the empirical equation:

$$\log(\epsilon_{Agg}/\epsilon_{IC}) = 20.4 - 0.0115\ T - 0.0045\ \sigma \qquad (4)$$

where T is in K, and the differential stress σ is in MPa. $\epsilon_{Agg}/\epsilon_{IC}$ must remain ≥ 1. Therefore, $\epsilon_{Agg}/\epsilon_{IC} = 1$ is here imposed when Eq. (4) gives values < 1. Note that, although empirical, Eq. (4) accounts for all dry and wet data with good consistency between studies. Combining Eqs. (2) and (4), a first-order estimate of the olivine aggregate strain rate can be calculated from the intracrystalline strain rate ϵ_{IC} (Eq. 3) through the following composite flow law:

$$\epsilon_{Agg} = \mathrm{Max}\left[1; 10^{\wedge}(20.4 - 0.0115\ T - 0.0045\ \sigma)\right] \times \epsilon_{IC} \qquad (5)$$

where Max[i;j] is the maximum of i and j, T is in K and σ is in MPa. Note that the effects of pressure, temperature, stress, oxygen fugacity, or hydrous conditions are accounted for in the intracrystalline flow laws (Eq. (3), supplementary materials, Table S2). In the following, we explore the implications for the upper mantle of the effect of pressure and temperature on intracrystalline vs. intergranular plasticity.

4. Discussion extrapolation to mantle conditions

Fig. 3a shows $\log(\epsilon_{Agg}/\epsilon_{IC})$ calculated along two oceanic geotherms (20 Ma and 80 Ma) for a differential stress $\sigma = 1$ MPa – i.e. a shear stress $\mu = 1/\sqrt{3}$ MPa, which is a reasonable value for the mid-to-deep upper mantle (Bürgmann and Dresen, 2008) – and along a classic continental geotherm [see Supplementary Information, Figure S1, see also Turcotte and Schubert (2002)] for $\sigma = 1$ and 50 MPa. The latter stress value is representative of shear zones in the coldest part of the lithosphere, and of experimental conditions. For this calculation, pressure was calculated with an upper mantle average density of 3.35 g/cm^3 (i.e. a 32.9 MPa/km vertical pressure gradient), and oxygen fugacity set at FMQ-2, which is reasonable for the upper mantle (Herd, 2008). We assumed wet condition for this plot (supplementary materials). Fig. 3a suggests that, like in experiments, deformation in the upper mantle is largely accommodated by intergranular plasticity, especially in the cold lithosphere where grain-to-grain interactions may fully dominate olivine plasticity. This may promote a significant

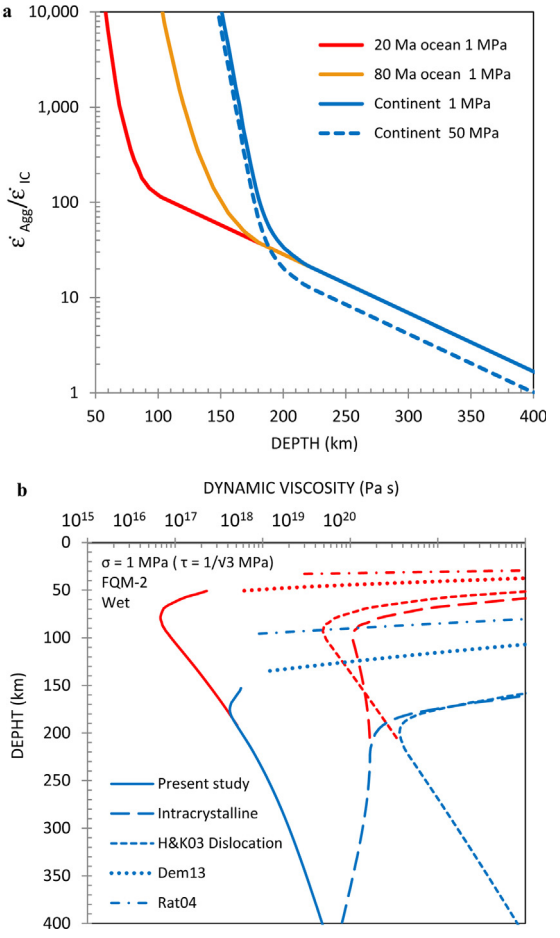

Fig. 3. a: ratio of the aggregate strain rate by the intracrystalline strain rate ($\epsilon_{Agg}/\epsilon_{IC}$) versus depth, as calculated from Eq. (4) assuming no effect of grain size, along 20-Ma (red) and 80-Ma (orange) oceanic geotherms, and a continental geotherm (blue) with a differential stress $\sigma = 1$ MPa (solid lines) and 50 MPa (dashed line); b: olivine aggregate dynamic viscosity as calculated along a 20-Ma oceanic geotherm (red lines) and a continental geotherm (blue lines) at 1 MPa stress and indicated conditions. The solid lines were obtained from Eq. (5) assuming wet conditions. The aggregate intracrystalline strain rate (ϵ_{IC}) is shown for comparison (Intracrystalline). Previously reported high-temperature and low-temperature flow laws for olivine polycrystals are also shown for comparison: H&K03 stands for Hirth and Kohlstedt (2003) dislocation creep law, assuming an activation volume of 12.8 cm^3/mol and an hydroxyl content $C_{OH} = 300$ ppm H/Si. Dem13 stands for Demouchy et al. (2013), and Rate04 for Raterron et al. (2004). See text for further explanation. The effect of the intergranular strain relaxation mechanism is apparent through the reduction of viscosity by a factor of ~ 100 (solid lines) at shallow depths relative to that obtained from Hirth and Kohlstedt's flow law or laws based on intracrystalline deformation (dashed lines). Do note, however, that such effect is probably reduced in the mantle because of larger grain sizes than in experiments. At deeper depths, the difference between the present law and that of Hirth and Kohlstedt (2003) is due to the pressure-induced change of dominant slip system in olivine.

weakening of the aggregate with respect to the strength calculated from classical flow laws.

Fig. 3b shows the viscosity of olivine aggregate along oceanic (20 Ma, red curves) and continental (blue curves) geotherms, as calculated using the composite flow law of Eq. (5) for a differential stress of 1 MPa. Wet conditions are

assumed when using Eq. (5), as well as for plotting Hirth and Kohlstedt (2003) dislocation creep flow law with hydroxyl content C_{OH} = 300 ppm H/Si. The intracrystalline strain rate calculated from Eq. (3) is shown for comparison, together with two low-temperature flow laws (Demouchy et al., 2013; Raterron et al., 2004). In both contexts, the composite flow law in Eq. (5) leads to viscosities about two orders of magnitude lower than those calculated using Hirth and Kohlstedt's dislocation creep flow law. Interestingly, in the shallow (cold) upper mantle, the composite flow law of Eq. (5) is in relatively good agreement with the low-temperature flow laws reported for olivine, thus captures the change in rheology between high-temperature and low-temperature plasticity. Changing the differential stress to 50 MPa does not significantly affect these results (Supplementary Information, Figure S2). At deeper depths (i.e. 400 km), the difference between the predictions of Eq. (5) and the dislocation creep law of Hirth and Kohlstedt (2003) is due to the pressure-induced change of dominant slip system in olivine (Raterron et al., 2012).

It should be emphasized here that polycristalline specimens in high-pressure experiments have small grain sizes, typically ranging from 1 to 50 μm, which increases significantly their surface versus volume ratio when compared to that of mantle rocks with estimated grain sizes ranging from tenths of millimetre to centimetres. This enhances grain-to-grain interactions, hence intergranular plasticity, in laboratory specimens and may artificially lower their strength with respect to that of mantle rocks. The results reported here (Eq. (5) and Fig. 2) may, thus, significantly overestimate how much strain can be accomodated by grain-to-grain interactions in the coarse-grain mantle. However, our results may apply more directly in the context of mantle shear zones, where grain size reduction weakens sheared peridotites (Skemer et al., 2011; Warren and Hirth, 2006).

5. Concluding remarks

According to our results and extrapolation, we conclude that olivine strain is mostly accommodated by deformation mechanisms involving grain-to-grain interactions at mantle pressures and temperatures, which results in a much weaker strength than that obtained when combining single crystal dislocation creep flow laws. Such a phenomenon was recently observed at low pressure (Tielke et al., 2016), but is much more marked at high-pressure where intergranular plasticity largely dominate deformation.

Uncertainties remain regarding the additional deformation mechanisms, present in aggregates and absent in single crystals, responsible for the measured low strength of aggregates with respect to that of single crystals. Several candidate mechanisms are mentioned in the introduction, such as disclinations, grain-boundary sliding, stress/strain percolation, etc., but our analysis does not allow us to favor one over another.

Furthermore, the empirical model presented here is extracted from deformation experiments carried out at high differential stresses on aggregates with small grain sizes compared to mantle conditions where stresses are much lower and grain sizes larger. Further investigation is necessary to quantify the effects of increasing grain size and decreasing stress on the parameters in Eq. (4). As mentioned above, one may speculate that, due to the larger grain sizes, intracrystalline mechanisms may accommodate more strain in the Earth's mantle than in experiments and, hence, reduce the effect of grain-to-grain interactions highlighted here. Another source of discrepancy when extrapolating the present results to mantle processes is the presence of secondary phases such as pyroxenes, garnet, and possibly partial melts in mantle peridotites, which are absent in the present laboratory specimens.

Keeping in mind the above reservations, let us however emphasize that olivine classical flow laws, whether assuming dislocation or diffusion creep, fail to explain the fast surface displacement observed by GPS after large earthquakes (e.g., Freed et al., 2010), which requires a much weaker strength for the lithosphere as the one we propose here. Also, the particularly deep weakening predicted here along a continental geotherm may provide an explanation for the elusiveness of the lithosphere – asthenosphere boundary beneath cratons (e.g., Eaton et al., 2009), since it should reduce the lithosphere – asthenosphere viscosity contrast. We thus conclude that grain-to-grain interactions are an important component of olivine plasticity at mantle pressures, and may likely contribute to the weakening of the Earth's upper mantle with respect to that calculated from classical flow laws for olivine.

Acknowledgements

This research was supported by the "Agence nationale de la recherche" (ANR) Grant BLAN08-2_343541 "Mantle Rheology". We thank two anonymous reviewers for their thoughtful insights, which helped improving the original manuscript. Part of the work was carried out while PR was serving at the National Science Foundation. Any opinion, findings, and conclusions or recommendations expressed in this material are those of the authors and do not necessarily reflect the views of the National Science Foundation.

Appendix A. Supplementary data

Supplementary data associated with this article can be found, in the online version, at https://doi.org/10.1016/j.crte.2018.10.001.

References

Bai, Q., Mackwell, S.J., Kohlstedt, D.L., 1991. High-temperature creep of olivine single crystals. Mechanical results for buffered samples. J. Geophys. Res. 96, 2441–2463.

Bollinger, C., Merkel, S., Raterron, P., Cordier, P., 2013. Olivine dislocation creep: revisiting experimental data to 8 GPa pressure. Phys. Earth Planet Inter. 228, 211–219.

Burnley, P.C., 2013. The importance of stress percolation patterns in rocks and other polycrystalline materials. Nat. Commun. 4, 2117, http://dx.doi.org/10.1038/ncomms3117.

Bürgmann, R., Dresen, G., 2008. Rheology of the lower crust and upper mantle: evidence from rock mechanics, geodesy and field observations. Annu. Rev. Earth Planet Sci. 36, 531–567.

Castelnau, O., Blackman, D.K., Lebensohn, R.A., Ponte Castañeda, P., 2008. Micromechanical modeling of viscoplastic behavior of olivine. J. Geophys. Res. 113, B09202, http://dx.doi.org/10.1029/2007JB005444.

Coble, R.L., 1963. A model for boundary diffusion controlled creep in polycrystallinematerials. J. Appl. Phys. 34 (6), 1679–1682.

Cordier, P., Demouchy, S., Beausir, B., Taupin, V., Barou, F., Fressengeas, C., 2014. Disclinations provide the missing mechanism for deforming olivine-rich rocks in the mantle. Nature 504, 51–56, http://dx.doi.org/10.1038/nature13043.

Demouchy, S., Tommasi, A., Boffa Ballaran, T., Cordier, P., 2013. Low strength of Earth's uppermost mantle inferred from tri-axial deformation experiments on dry olivine crystals. Phys. Earth Planet. Inter. 220, 37–49.

Durham, W.B., Mei, S., Kholstedt, D.L., Wang, L., Dixon, N.A., 2009. New measurement of activation volume in olivine under anhydrous condition. Phys. Earth Planet Inter. 172, 67–73.

Eaton, D.W., Darbtshire, F., Evans, R.L., Grütter, H., Jones, A.G., Yuan, X., 2009. The elusive lithosphere-asthenosphere boundary (LAB) beneath cratons. Lithos 109, 1–22.

Freed, A.M., Herring, T., Bürgmann, R., 2010. Steady-state laboratory flow laws alone fail to explain post-seismic observations. Earth Planet Sci. Lett. 300, 1–10.

Frost, B.R., 1991. Introduction to oxygen fugacity and its petrologic importance. In: Lindsley, D.H. (Ed.), Reviews in Mineralogy. Oxide Minerals: Petrologic and Magnetic Significance, Volume 25, Mineralogical Society of America, New York, pp. 1–10.

Frost, H.J., Ashby, M.F., 1982. Deformation Mechanisms Maps: The Plasticity and Creep of Metals and Ceramics, first ed. Pergamon, Oxford/New York/Sydney.

Girard, J., Chen, J., Raterron, P., Holyoke III., C.W., 2013. Hydrolytic weakening of olivine at mantle pressure: evidence of [100](010) slip system softening from single crystal deformation experiments. Phys. Earth Planet Inter. 216, 12–20.

Hansen, L.N., Zimmerman, M.E., Kohlstedt, D.L., 2011. Grain-boundary sliding in San Carlos olivine: flow law parameters and crystallographic-preferred orientation. J. Geophys. Res. 116, B08201, http://dx.doi.org/10.1029/2011JB008220.

Hansen, L.N., Zimmerman, M.E., Kohlstedt, D.L., 2013. Laboratory measurements of viscous anisotropy of olivine aggregates. Nature 492, 415–418.

Herd, C.D.K., 2008. Basalts as probes of planetary interior redox state. Rev. Mineral. Geochem. 68, 527–553.

Hilairet, N., Wang, Y., Sanehira, T., Merkel, S., Mei, S., 2012. Deformation of olivine under mantle conditions: an in situ high-pressure, high-temperature study using monochromatic synchrotron radiation. J. Geophys. Res. 117, B01203, http://dx.doi.org/10.1029/2011JB008498.

Hiraga, T., Miyazaki, T., Tasaka, M., Yoshida, H., 2010. Mantle superplasticity and it self-made demise. Nature 468, 1091–1094, http://dx.doi.org/10.1038/nature09685.

Hirth, G., Kohlstedt, D.L., 1995. Experimental constraints on the dynamics of partially molten upper mantle 2: deformation in the dislocation creep regime. J. Geophys. Res. 100B8, 15441–15449.

Hirth, G., Kohlstedt, D.L., 2003. Rheology of the upper mantle and the mantle wedge: a view from the experimentalists. In: Eiler, J. (Ed.), Inside the Subduction Factory. Geophys. Monogr. Ser., AGU, Washington, DC, pp. 83–105.

Keefner, J.W., Mackwell, S.J., Kohlstedt, D.L., Heidelbach, F., 2011. Dependence of dislocation creep of dunite on oxygen fugacity: implications for viscosity variations in Earth's mantle. J. Geophys. Res. 116, B05201, http://dx.doi.org/10.1029/2010JB007748.

Kohlstedt, D.L., 2006. The role of water in high-temperature rock deformation. Rev. Mineral. Geochem. 62, 377–396.

Mackwell, S.J., Kohlstedt, D.L., Paterson, M.S., 1985. The role of water in the deformation of olivine single crystals. J. Geophys. Res. 90, 11319–11333.

Ohuchi, T., Kawazoe, T., Higo, Y., Suzuki, A., 2017. Flow behavior and microstructures of hydrous olivine aggregates at upper mantle pressures and temperatures. Contrib. Mineral. Petrol. 172, 65, http://dx.doi.org/10.1007/s00410-017-1375-8.

Raterron, P., Wu, Y., Weidner, D.J., Chen, J., 2004. Low-temperature olivine rheology at high-pressure. Phys. Earth Planet Inter. 145, 149–159, http://dx.doi.org/10.1016/j.pepi.2004.03.007.

Raterron, P., Amiguet, E., Chen, J., Li, L., Cordier, P., 2009. Experimental deformation of olivine single crystals at mantle pressure and temperature. Phys. Earth. Planet Inter. 172, 74–83.

Raterron, P., Chen, J., Geenen, T., Girard, J., 2012. Pressure effect on forsterite dislocation slip systems: Implications for upper-mantle LPO and low viscosity zone. Phys. Earth Planet Inter. 188, 26–36.

Skemer, P., Sundberg, M., Hirth, G., Cooper, R., 2011. Torsion experiments on coarse-grained dunite: implications for microstructural evolution when diffusion creep is suppressed. Geol. Soc., London Spec. publ. 360, 211–233, http://dx.doi.org/10.1144/SP360.12.

Tielke, J.A., Hansen, L.N., Tasaka, M., Meyers, C., Zimmerman, M.E., Kohlstedt, D.L., 2016. Observation of grain size sensitive power law creep of olivine aggregates over a large range of lattice-preferred orientation strength. J. Geophys. Res. Solid Earth 121, 506–516, http://dx.doi.org/10.1002/2015JB012302.

Turcotte, D.L., Schubert, G., 2002. Geodynamics, second ed. Cambridge University Press, New York, USA (456 p.).

Warren, J.M., Hirth, G., 2006. Grain size sensitive deformation mechanisms in naturally deformed peridotites. Earth Planet Sci. Lett. 236, 438–450.

Wendland, R.F., Huebner, J.S., Harrison, W.J., 1982. The redox potential of boron nitride and implications for its use as a crucible material in experimental petrology. Am. Mineral. 67, 170–174.